Synthetic Notch Activation Patterns in a Proliferating Tissue

Jonathan E. Dawson[1], Abby Bryant[2], Trevor Jordan [2], Simran Bhikot[2], Shawn Macon[1,2], Breana Walton[2], Amber Ajamu-Johnson[2], Paul D. Langridge [2*†], Abdul N. Malmi-Kakkada[1*†]

[1]Department of Physics and Biophysics, Augusta University, Augusta, GA 30912, USA

[2]Department of Biological Sciences, Augusta University, Augusta, GA 30912, USA

(Dated: 31 October 2023)

Cell-cell communication through direct contact is essential during fundamental biological processes such as tissue repair and morphogenesis. Synthetic forms of contact-mediated cell-cell communication can generate custom gene expression outputs, making them valuable for tissue engineering and regenerative medicine. To precisely control the location and timing of synthetic signal outputs in growing tissues, it is necessary to understand the mechanisms underlying its spatiotemporal patterns. Towards this goal, we combine theory and experiments to study patterns of synthetic Notch (synNotch) activation - a custom synthetic gene circuit that we implement within *Drosophila* wing imaginal discs. We show that output synthesis and degradation rates together with cell division are the key minimal parameters that predict the heterogeneous spatiotemporal patterns of synNotch activation. Notably, synNotch output forms a graded exponential spatial profile that extends several cell diameters from the signal source, establishing evidence for signal propagation without diffusion or long range cell-cell communication. Furthermore, we discover that the shape of the interface between ligand and receptor cells is important in determining the synNotch output. Overall, we elucidate key biophysical principles that underlie complex emergent spatiotemporal patterns of synNotch output in a growing tissue.

*Corresponding authors:plangridge@augusta.edu, amalmikakkada@augusta.edu

†Senior co-authors

INTRODUCTION

Synthetic biology combines biological and engineering principles to regulate cellular processes and is emerging as an important area of biomedical research. Synthetic means of manipulating interactions between cells to control tissue behavior has enormous therapeutic potential since it would allow natural developmental programs governing growth, differentiation or cell death to be deployed at customized times or locations[1–3]. Such engineered intercellular communication could facilitate the initiation of natural cellular processes that sculpt tissue into custom shapes required for tissue engineering or regenerative medicine applications[4]. At the same time, synthetic approaches offer an opportunity to elucidate principles governing the development of native tissues[5] as synthetic programs can mimic native ones for the spatial patterning of cellular differentiation and growth[6–10]. However, deploying synthetic signals *in vivo* to produce a desired response remains a major challenge, and little is known about the capacity of current technologies to achieve this goal.

A key challenge is to design synthetic signaling systems to create an output at precise times and locations, such that cells gain positional information and regulate cell-fate decisions[11–13] akin to how morphogen diffusion-driven concentration gradients regulate cell behaviors[14,15]. Recent studies on the spatiotemporal patterning of output in contact-mediated signaling circuits have mainly focused on *in vitro* implementations in fixed domains[16,17] rather than within rapidly proliferating tissues relevant during both embryo and tumor growth[18]. Knowing how tissue growth with consequent changes in cell number and spatial rearrangement of signal-sending and receiving cells may alter such engineered responses is an important next step. To address this challenge, we elucidate the biophysical properties of *in vivo* cell-cell signaling in growing tissues by developing a synthetic tool kit for use in the developing *Drosophila* wing imaginal disc together with a minimal mathematical model. We verify our predictions by comparing with *in vivo* synNotch output quantifications and discover that cell-cell signaling output coupled with cell division in growing tissues set up an emergent graded spatial output profile. Rather than being restricted only to the synNotch cells at the interface, we find that the output extends into the clone, depending on the rates of output biosynthesis, degradation and cell division. Additionally, we ascertain that clone shape is important in determining juxtacrine signaling output.

RESULTS

A synNotch circuit in growing *Drosophila* epithelia leads to heterogeneous output patterns

The *Drosophila* wing imaginal disc is a long-standing and powerful model epithelial tissue within which cell fate patterning and growth are exceptionally well understood[19–21] and with established techniques for controlling and monitoring signaling events[22,23]. It undergoes extensive proliferation[24] making it ideal for our purposes to study the impact of tissue growth on signal output. During development, the wing disc grows from ∼5-40 cells to ∼40,000 cells within a time span of 3 days where signaling events can be conveniently measured[25]. Synthetic cell-cell communication provides a simplified juxtacrine signaling system for analysis *in vivo* since the signal inputs and outputs can be customized and operate orthogonally[26,27] to endogenous signal systems that govern normal tissue growth.

Given these advantages, we implement a synthetic contact-mediated signaling system based on the Notch receptor, an important and pervasive signaling system in the development of all animals (see Materials and Methods Section 1)[28,29]. The Notch receptor and its ligands, such as the *Drosophila* ligand Delta, are single-pass transmembrane proteins. Delta, presented on the cell surface, binds to the ectodomain of Notch on neighboring cells and this physical interaction activates the receptor by inducing proteolytic cleavage of Notch. This results in the intracellular domain moving to the nucleus to act as a transcriptional activator of Notch target genes, such as Cut (as described in detail, Fig 1(A)). synNotch uses the same activation mechanism but with parts of native Notch replaced with heterologous functional domains (Fig 1(B)). Previously, forms of Delta with the extracellular domain replaced with Follicle Stimulating Hormone (FSH) were shown to activate chimeras of Notch with the FSH receptor (FSHR) binding regions[30]. To produce a functional synNotch receptor, we modified FSHR-Notch by introducing heterologous cleavage and transcription factor domains, to obtain FSHR-synNotch that when activated induces of expression of a form of GFP (see Fig 1(B)) and deployed it in the *Drosophila* wing imaginal disc.

As in previous work with FSHR-Notch, the proteins were overexpressed with the UAS/Gal4 system in the *Drosophila* wing disc in signal sending or signal receiving populations using Mosaic Analysis by Promoter Swap (MAPS)[31]. This technique subdivides

the third instar wing disc into clonal populations of cells expressing FSH-Delta (referred to as 'ligand clones') and cells expressing FSHR-synNotch (referred to as 'synNotch clones'). Expressing these components does not change Cut expression nor the development of the wing (see Supplementary Information (SI) Section 1 and Fig. S1), indicating that FSHR-synNotch operates orthogonally to native Notch.

We visualize the synNotch output at points of contact between ligand and synNotch clones in the third instar wing disc (referred to here simply as 'wing') (Fig 1(B)). Our *in vivo* observations provide two important insights. Notably, the GFP output is detected in synNotch clones not in contact with the ligand or FSH-Delta clone (arrowheads in Fig. 1(B)). Moreover, the GFP intensity along the interface is not uniform (cells with different intensities are marked with arrows in Fig 1(B)). This suggests that in proliferating epithelial tissues the synNotch response is variable and not restricted to those synNotch cells in direct contact with ligand cells as might be expected with a juxtacrine signal. Hence, to understand and control the signal output patterns in proliferating tissues, we implement a minimal computational model as we discuss further below.

Computational model predicts that synNotch output depends on clone shape

From a physical perspective, embryonic tissues are growing active materials with variations in geometry and mechanical properties that impact cell behaviors [32–35]. To successfully control and predict the time, location, and extent of synNotch outputs within growing tissues, it is necessary to understand how cell proliferation changes the shape of the ligand-synNotch interface (Fig. 1(C i,ii)). To address this, we developed a novel vertex-based[36,37] mathematical model with mechanochemical coupling between vertex dynamics and intracellular synNotch output (see Fig. 1(D) and Materials and Methods Sections 2-4 for details). We hypothesize that the synNotch output (G_α [arbitrary units] as a function of time (t)) increases with larger contact lengths between synNotch and ligand cells (Fig. 1(D-ii))[16] (Materials and Methods Section 3). The *in silico* tissue consists of two cell types: (i) synNotch cells with no output (Fig. 1(D), gray), but which can produce GFP upon synNotch activation (Fig. 1(D-i), green) while in contact with (ii) ligand cells (Fig. 1(D), blue). The output strength is visualized by a green color scale, with black color denoting no output and bright green color representing high output (Fig. 1(D-ii)). In each cell, GFP is continuously

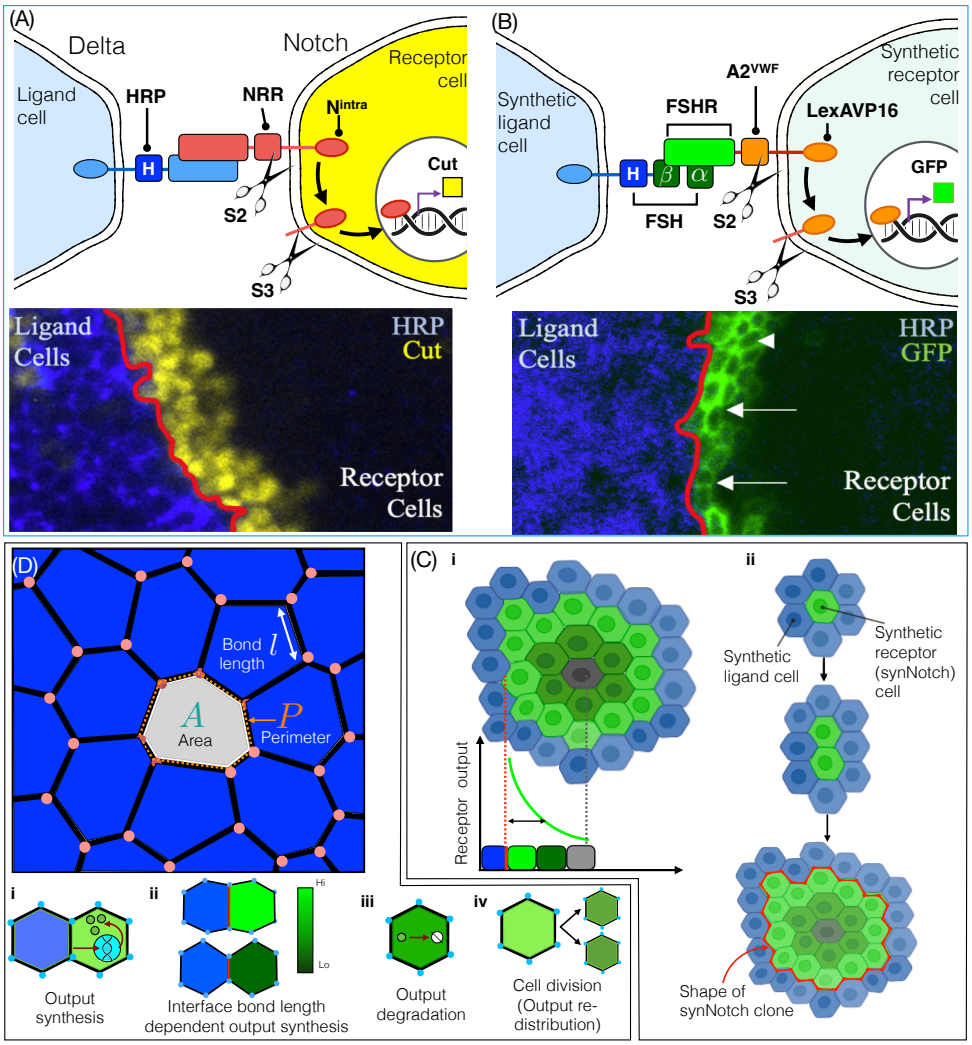

FIG. 1: Caption on the next page

degraded at the rate D [per hour (h^{-1})] (Fig. 1(D-iii)).

A cell divides along its short axis when its area doubles with the total amount of GFP distributed equally between the two daughter cells (Fig. 1(D-iv)) (see Materials and Methods Section 4 for details and Table (1) for a list of relevant simulation parameters). Repeated cycles of cell growth and division lead to clone size expansion over time, as shown in Fig. 2(A) and SI Movies 1-3 (snapshots of an expanding synNotch clone at 3 distinct timepoints are highlighted with yellow bars in the inset). Tissue growth leads to spatially heterogeneous GFP expression among cells, as predicted by the model. In general, output intensity is higher at the border cells compared to the clone interior, with marked variation in the GFP intensity even among border cells. In these respects, the *in silico* prediction reflects the spatial heterogeneity in the output observed in confocal images of FSHR-synNotch clones

FIG. 1: ***In vivo* synNotch activation exhibits heterogeneous output patterns in a growing epithelial tissue. (A)** Top: Schematic of native *Drosophila* Delta binding to Notch on the surface of a signal-receiving receptor cell, which induces the S2 cleavage of the Negative Regulatory Region (NRR). After S2 cleavage, the intramembrane S3 cleavage allows nuclear access of the intracellular domain (N^{intra}), and activation of target genes such as *Cut*. Bottom: Confocal image of ectopic *Cut* expression (native output) in the nuclei of wing cells overexpressing Notch (receptor) adjacent to cells overexpressing Delta (ligand). **(B)** Top: Schematic of FSHR-synNotch activation. The synNotch activation mechanism is the same as native Notch, although the following components of the receptor and ligand differ. The Delta extracellular domain was replaced with the β-subunit of follicle stimulating hormone (FSH), and FSHα was co-expressed to reconstitute the composite FSH ligand (FSH); the ligand binding region of the Notch ectodomain was replaced by the FSH receptor ectodomain (FSHR); the NRR was replaced with the A2 force sensitive domain; and the intracellular domain was replaced with the lexA-VP16 transcription factor. S2/S3 cleavage and movement of the intracellular domain to the nucleus proceeds as for native Notch, but in this case the target gene activated is the lexAop rCD2-GFP transgene (referred to here as GFP). Bottom: Confocal image of GFP (output) at the surface of wing cells overexpressing FSHR- synNotch (synNotch receptor) that are adjacent to cells overexpressing FSH-Delta (synthetic ligand), although the intensity of GFP varies (arrows) and extends several cell diameters from the clone interface (arrowheads). **(C)** In this work we focus on variations in synNotch output patterns in a growing tissue, leading to spatial gradients in output across the receptor clone. **(D)** Schematic of the two-dimensional (2D) computational vertex model for synNotch induced gene expression. Cells are represented by polygons (composed of vertices shown as colored dots) with a preferred area A_0 and preferred perimeter P_0. The cell shape is characterized by an energy function that describes the balance between cell area compressibility and cell perimeter contractility (see Materials and Methods Section 2 for further details). Our model takes into account biological processes governed by different timescales, (i-ii) cell-cell contact length dependent GFP output synthesis rate, (iii) GFP degradation rate and (iv) cell division rate. Cell division redistributes the total GFP of the parent cell equally between the two resulting daughter cells (iv).

(Fig. 1(B)). Moreover, we generated *in vivo* clones allowing for $24, 48$ and $72h$ of proliferation into wing development. As predicted, cells in the clone interior lack strong GFP expression at 72 hours (Figs. 2 (B-D)).

We anticipate that cell growth and division can lead to highly dynamic contact interface lengths between synNotch and ligand cells, leading to complex clonal shapes and heterogeneous output patterns. For a more stringent test, we quantify the clone shape using the circularity parameter, $C = 4\pi A/P^2$, which equals 1 for a circle and approaches 0 for highly distorted clone shapes (Fig. 2(F), where A, P are the clone area and perimeter respectively). Notably, our model predicts that the total GFP output is inversely proportional to the clone circularity (see Materials and Methods Section 5). In agreement with our predictions, the GFP output in the synNotch cells at the interface depends strongly on the clone shape (Fig. 2(G)) with low output when the clone shape is highly circular and higher output for highly irregular shapes. Therefore, we surmise that clone shape is important in determining

cell-cell contact-based signal output patterns.

By incorporating cell mechanical properties and tissue growth, our new model not only recapitulates general spatial synNotch output patterns, but also quantitatively predicts the impact of clonal shape. Because both modeling and observations suggest a key role for clonal shape in synNotch output, we next sought to understand output spatial features across and along the clonal boundary.

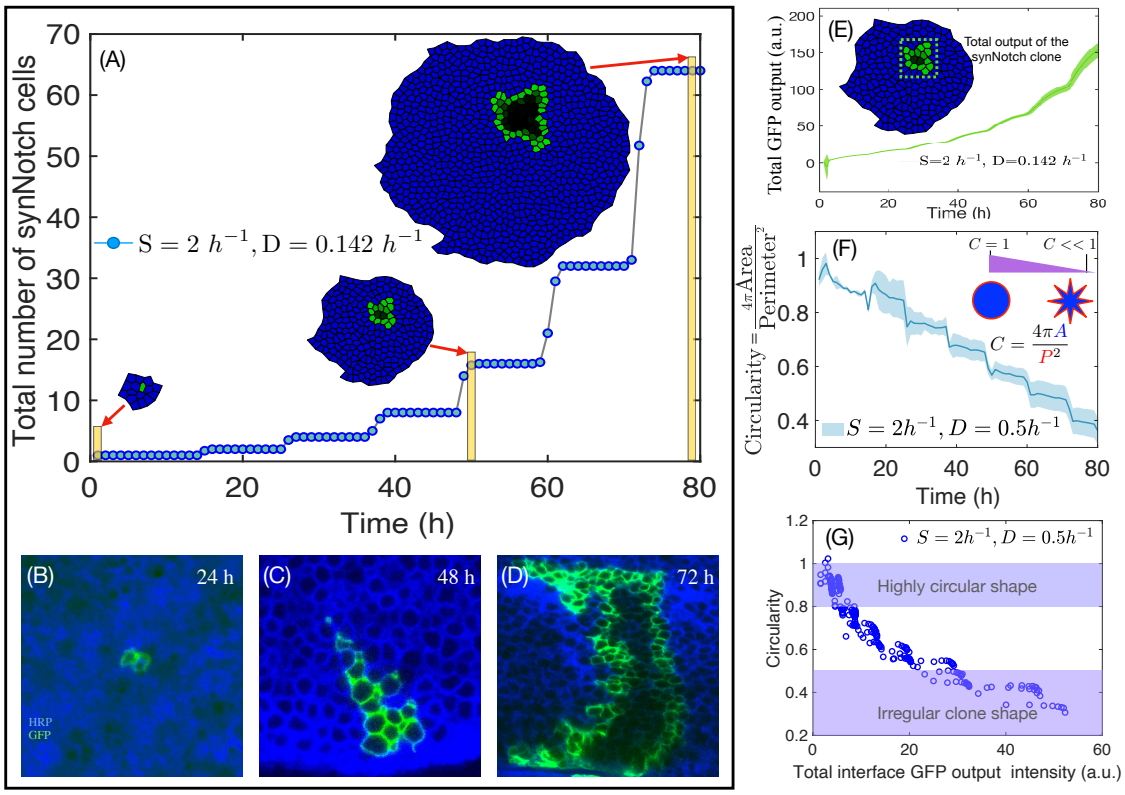

FIG. 2: Caption on the next page.

Output signal propagation exhibits exponential decay and extends up to 3 cell diameters from the clonal interface *in vivo*

Our *in silico* predictions and measured synNotch activation *in vivo* together suggest that the output response spreads significantly farther away from the signaling interface. This is similar to a spatial morphogen gradient with variation in the concentration of transcription factors or signaling molecules across a field of cells[38,39]. While diffusion establishes morphogen spatial gradient across tissues, whether localized cell-cell contact based signaling can produce a similar output gradient is unclear.

FIG. 2: **Clone shape determines emergent differences in spatial synNotch output patterns in growing tissues. (A)** As the tissue expands due to multiple cell division events, the number of synNotch cells increases over time and take on complex clone shapes. The initial state of the tissue consists of multiple ligand cells (blue) and one Notch cell (green). **(B-D)** Confocal images of distinct *Drosophila* wing imaginal discs at 24, 48 and 72 h after clonal generation of populations of FSHR-synNotch (uncolored and green) and FSH-Delta (blue) expressing cells by mitotic recombination. At 24 h after recombination, small clones of only a few cells are visible and all express GFP. Such clones appear larger at 48 h with all cells expressing GFP. By 72 h the FSHR-synNotch clone is large enough that significant number of cells are far from FSH-Delta cells and do not express GFP. Qualitatively the images appear similar to modelled clones at similar time points, as shown in (A). **(E)** The total GFP expression in the whole synNotch clone increases as a function of time for a fixed value of output synthesis and degradation rates. The data is averaged over 3 simulation runs. The shaded area represents the standard deviation here and henceforth. **(F)** The shape of the synNotch clone evolves to a highly irregular shape as quantified by the circularity parameter. A perfect circle has a circularity of 1 and a highly distorted or elongated shape has a circularity approaching 0 (see Inset). **(G)** Total GFP output intensity in the interface synNotch cells is inversely proportional to the clone circularity indicative of the strong influence of the synNotch clone shape on the GFP output.

Our observations point to the output degradation rate (D) as an important parameter in controlling the spatial gradient of the GFP output across the synNotch cell clone. In the model, we vary D from $0 - 0.5h^{-1}$ including the physiologically relevant value of $D \sim 0.142h^{-1}$ [40,41] keeping S fixed at $2h^{-1}$. We observe generally that the border synNotch cells in contact with the ligand cells have high intensity of GFP output (bright green), which gradually weaken (light green to gray) towards the center of the clone (SI Fig. S2(A-B)) - a spatial pattern strongly dependent on D. For small D, synNotch cells not directly at the clone border express significant levels of GFP (see SI Fig. S2(A)). At higher values of D, a "donut"-like pattern emerges with little to no GFP (gray) expression at the clone interior and high GFP levels at the periphery (see SI Fig. S2(B-C)). This suggests that the extent to which GFP output is lost in the synNotch clone interior is largely determined by D.

To quantify the GFP output gradient, we focused on the spatial region traversing the boundary and interior of the synNotch clone in Fig. 3(A). The spatial output profile has a peak at the clone boundary, and a gradient with lower GFP in the clone interior (see Fig. 3(B)). With increasing D, the output decay is steeper in Fig. 3(C). Moreover, the GFP intensity normalized to the synNotch cell at the interface (Fig. 3(C)) is well described by an exponential of the form e^{i/i^*}, where i is the cell index and i^* is the characteristic number of cells from the border over which the output amplitude decays by $1/e$. For $D = 0, i^* \sim 2$, implying that a significant drop in output intensity occurs beyond 2 cells from

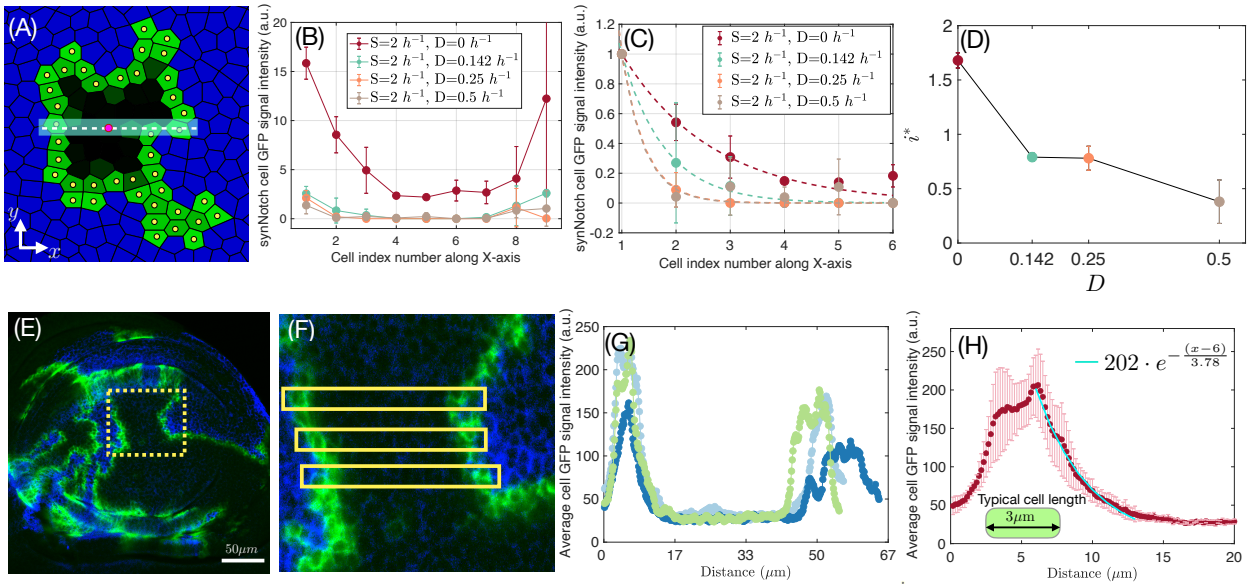

FIG. 3: **synNotch output decays exponentially away from the clonal interface depending on the output degradation rate (A)** The spatial profile of synNotch output (i.e. GFP signal intensity), *in silico*, across the receptor cell clone (see white dashed line) at late times, $t = 80h$. We first identify synNotch cells located within a narrow horizontal band that passes through the clone center of mass, i.e., $|y_\alpha - y_{CM}| < 2\ \mu m$, where y_α is y coordinate of a synNotch cell α and y_{CM} is the y component of the center of mass (R_{CM}) of the synNotch clone (see pink dot marking the center and dashed line marking the horizontal strip). $\vec{R}_{CM}$ is defined as $\vec{R}_{CM} = 1/N \sum_\alpha^N \vec{r}_\alpha$, where N is the total number of synNotch cells and $\vec{r}_\alpha$ is the coordinate of a synNotch cell α. **(B)** Simulation results for the GFP signal intensity along the x axis across the receptor cell clone for fixed output synthesis rate and varying output degradation rate D (see figure legend). Each data point is the mean of three independent simulation runs. Error bars show the standard deviation here and henceforth. **(C)** GFP signal intensity, shown in (B), rescaled by the GFP signal intensity of the first synNotch cell from the left. Rescaled data is fit by an exponentially decaying function (dashed lines) of the form e^{x/i^*}. **(D)** The value of i^*, obtained from the fits decreases with D. **(E)** Confocal image of GFP (green) at the surface of *Drosophila* wing cells overexpressing FSHR-synNotch that are adjacent to FSH-Delta cells (blue). **(F)** Spatial profile of GFP output was quantified along three different horizontal sections across the clone as shown by the three yellow boxes. GFP intensity is averaged over the box width. **(G)** Spatial GFP output profile at three different locations across the synNotch clone. The origin is the left end of the yellow boxes shown in (F). The two peaks correspond to the interface region between ligand and synNotch receptor cells. **(H)** Average of the three spatial profiles of GFP output near the interface. Magenta-filled circles represent the mean, and the error bars show the standard deviation. The average data is fit by an exponential function of the form Ae^{x/i^*} (turquoise colored line). $i^* = 3.78\ \mu$m. The average diameter of a synNotch cell is shown in the inset equalling 3μm. Further extensive analysis of multiple wing discs (see SI Fig. S3) confirms this result.

the clonal interface. For $D = 0.5h^{-1}, i^* \sim 0.5$, indicating that the output intensity decays substantially within one cell layer from the boundary (see Fig. 3(D)). By measuring the cell diameter from the *in vivo* images, we can predict the propagation of the GFP output into the synNotch clone in terms of the characteristic distances.

Our results imply that the output degradation rate is an important parameter in determining the extent of output propagation. By fitting an exponential function to the spatial output, we can deduce the signal output decay rates *in vivo*. Conversely, by fixing D, we can in principle quantify the synthesis rate(S) on the basis of the output spatial profile. As S is a complex multi-scale parameter dependent on molecular scale factors such as the translocation of the synthetic transcriptional activator to the nucleus as well as cell-cell junction mechanical properties, this result will be useful for improving the predictability of synthetic gene circuit outputs *in vivo*.

Next, to validate the computational model, we compare our model predictions with FSHR-synNotch activation *in vivo* using the GFP fluorescence intensity in synNotch clones adjacent to ligand clones. The GFP output intensity at three different sections of the tissue, Fig. 3(E-F), show a clear peak at the boundary and a gradient with lower intensity towards the clone center. This is similar to our *in silico* predictions, compare Figs. 3(B) and (G). The average GFP intensity profile is well described by an exponential function, Fig. 3(H). The fit revealed that the spatial gradient of GFP is characterized by a distance scale of ~ 1.5 cell diameters. This result is significant, as we would expect the output to be strictly confined to cells that are directly in contact with the signal-sending ligand cells. Instead, we find a spatially graded signal output that on average propagates more than one cell diameter from the boundary into the receptor clone.

To analyze this further, we selected clones with clear GFP propagation and measured the expression profile of GFP and how far GFP signal extended from the signal interface (SI Fig. S3). This was done by fitting an exponentially decaying function (as in Fig. 3(H)) to the measured GFP intensity from the interface to the location where GFP intensity profile plateaued at low-intensity values (Fig. S3(A4-E4)). We obtained the characteristic decay length of the GFP output into the clone from each *in vivo* experiment, (see blue lines in SI Fig. S3(A4-E4)). Notably, the output signal propagates as far as 3 cell diameters away from the clonal interface (in 3 out of 5 experiments). On average it extends 2 cell diameters into the receptor clone (see dashed line in Fig. S3(F)). Overall, the GFP output is detected multiple cell diameters away from the ligand-receptor cell boundary *in vivo*.

Because both modeling and observations suggest a key role for the output degradation rate for signal propagation into the clone, we next sought to understand whether S, D affects output along the clonal boundary.

Output response in synNotch cells along the clonal interface is highly spatially uncorrelated

Notch signal output increases with the contact length between the signal-sending and signal-receiving cells which in turn links cell morphology and fate determination[16]. As the tissue expands due to cell growth and division, it is likely that there will be variations in the cell bond length of individual synNotch cells which are in contact with the ligand cells. We hypothesize that these temporal variations in interface contact length account for the heterogeneous synNotch output along the interface that we noted both *in vivo* and in our computational model (as in Fig. 2(H-J)). To test this, we quantified the GFP output of synNotch cells along the interface *in silico* (see Fig. 4(A)). To do this in a consistent manner, we assign angular positions θ_k to border synNotch cells with the center of the synNotch clone marked with pink dot in Fig. 4(A). In general, we observe large fluctuations in the GFP intensity in cells along the border. The fluctuation amplitude depends on D, although at all levels of D, the fluctuations persisted (Fig. 4(B)).

We quantified the output heterogeneity along boundary cells using the GFP intensity angular correlation function,

$$Corr(\theta_k) = \Sigma_{i,j}\delta(\theta_k - (\theta_i - \theta_j))[(G(\theta_i) - \langle G\rangle)(G(\theta_j) - \langle G\rangle)], \tag{1}$$

where $G(\theta_i)$ is the GFP intensity in cell i whose angular position is θ_i and $i, j = 1...N_b$ are the indices for the total number of boundary cells (N_b). $\delta(z) = 1$ if $z = 0$, and 0 otherwise. $\langle G\rangle$ is the mean GFP intensity along the boundary. The autocorrelation function defined in Eq. (1) measures the correlation between signal intensities in cells along the border. The decay in the correlation function quantifies the similarity in the GFP output between any two synNotch cells along the boundary, with quicker (slower) decay denoting low (strong) correlation. We compute $Corr(\theta_k)$ for both varying D (Fig. 4(C)) and varying synthesis rate S (Fig. 4(D)). In both cases, the correlation function exhibits fast decay with respect to the change in angular positions (θ_k) implying that cell-to-cell variations in the GFP output at the synNotch clone border are independent of the rates of both GFP synthesis S and degradation D rates. Therefore, unlike the output propagation into the clone that is largely dependent upon decay rates, output spatial pattern along the clone boundary shows no dependence on either S or D. This is consistent with the prediction that the variability in cell-cell contact length along the border cells determines the output response pattern.

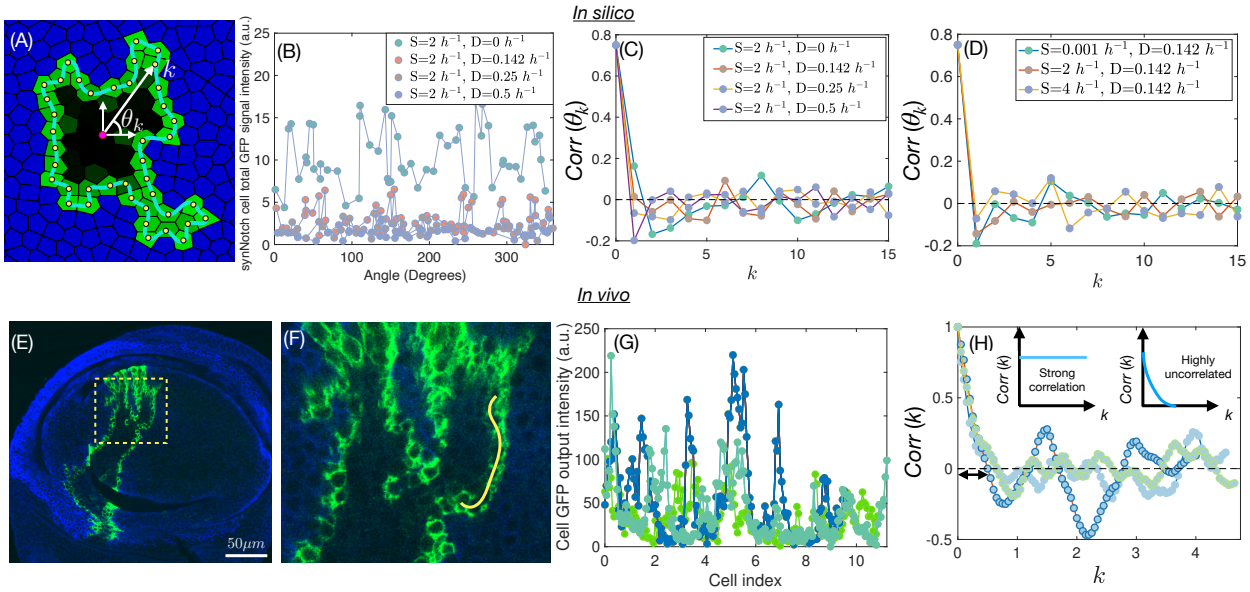

FIG. 4: **Output along the boundary of synNotch cell clone is highly spatially uncorrelated.** **(A)** The spatial profile of GFP output in synNotch receptor cells quantified along the border cells at the synthetic receptor-ligand expressing cell interface at $t = 80h$. The angular position of a border synNotch cell k is obtained from coordinates of the cell center (x_k, y_k) and the center of mass of the synNotch cell clone (x_{CM}, y_{CM}) as, $\theta_k = \tan^{-1}(\frac{y_k - y_{CM}}{x_k - x_{CM}})$. **(B)** Total GFP signal intensity in the border synNotch cells as function of the cell angular position θ_k for a fixed value of $S = 2h^{-1}$ and different values of $D = 0h^1, 0.142h^1, 0.25h^1, 0.5h^1$. **(C,D)** Autocorrelation function of the of GFP signal intensity in the border synNotch cells for (C) fixed $S = 2h^{-1}$ and varying D, and for (D) fixed $D = 0.142h^{-1}$ and varying S. Fast decay in the output intensity fluctuation correlation is characteristic of the high variability in the output between synNotch cells at the border. **(E)** Fluorescence microscopy image of *in vivo* FSHR-synNotch activation in the *Drosophila* wing imaginal disc. Green color shows the fluorescence intensity of the GFP output in synNotch cells, and the blue color marks ligand cells. **(F)** Zoom-in image from panel (E) showing the spatial profile of GFP output quantified along the border of synNotch clone (along the yellow line). **(G)** GFP output intensity, rescaled to the typical cell size of $3\mu m$, along the border of the synNotch clone. The three curves represent different boundary segments. **(H)** Autocorrelation analysis of fluctuations in the GFP output intensity along the border of the synNotch clone shows rapid decay to zero. This indicates large fluctuations in GFP output along the cells at the border. Inset plots show correlation as a function of cell index when there is strong correlation in output versus a highly uncorrelated scenario.

The GFP output intensity in synNotch cells *in vivo* along a section of the clone boundary is shown in Fig. 4(E) and the zoom-in image in Fig. 4(F) in multiple wing discs. The GFP intensity profiles are quantitatively similar to the simulations, with large fluctuations along the border of the synNotch clone, Fig. 4(G). Note that there is a difference in the GFP quantification between the simulation and *in vivo*. In the simulations, we track GFP output per cell while in the experiments we track it at the cell border since GFP is at the cell surface. Because we average over a line of finite thickness in the *in vivo* quantifications, we are able to

make a direct comparison with the simulations. By performing the autocorrelation analysis of the experimental data according to Eq. (1), we observe that the GFP output correlation decays rapidly (Fig. 4(H)). $Corr(k) \sim 0$ within 1 cell neighbor, in agreement with our model predictions. Here, we rescale the distance along the synNotch clone border into cell index (k) based on cell size quantification from *in vivo* images (20 pixels = $3\mu m$ = 1 cell diameter). The excellent agreement in the spatial correlation of the output intensity between simulation predictions and experiments enable us to conclude that variations in cell- cell contact lengths could be the primary contributor to the heterogeneity in the output intensity along the border synNotch cells.

Our *in vivo* experiments show that the GFP intensity profile along the ligand-receptor interface is characterized by rapidly decaying spatial correlations and strong fluctuations. Our model suggests that this behavior could arise due to heterogeneity in the interface contact lengths between synNotch and ligand cells. There are two prominent sources of cell-cell contact length heterogeneity, (i) stochastic cell area growth, and, (ii) random orientation of cell division. As both these processes are influenced by tension along the cell-cell junction and is regulated by the subcortical network of cell acto-myosin, our work provides a tool to study and predict the influence of cell bond tension on spatial patterning of juxtacrine signal output. Depending on the orientation of cell division, a responding daughter cell at the clonal interface may be displaced from the interface such that it either completely loses contact with the ligand expressing cells or continue to maintain contact. Moreover, cell divisions could also lead to increasing, decreasing or loss of contact between signal-sending/receiving cells, with each scenario influencing the level of synNotch output. In proliferating tissues where cell division axes are oriented randomly, as in the fly wing[42], there is likely to be emergent variation in the juxtacrine signal output. This would need to be factored in when engineering a persistent zone of cells that are required to respond uniformly to synthetic gene circuits. For instance, feedback circuits might be necessary to refine a precise region of persistent response following an initial signal activation in multiple cells within tissues. In fact, positive feedback is common to many signaling pathways and occurs during native Notch activation, for example, to form the boundary between dorsal and ventral cell populations that will form the margin of the fly wing after pupation[43].

Large variations in cell sizes lead to highly heterogeneous synNotch output response *in vivo*

We anticipate that the cell-cell contact length is a highly dynamic variable that changes due to cell shape fluctuations coupled with cell growth and division events. Within growing tissues, variations in cell-cell contact length are likely important in determining both the magnitude and the spatial gradient of the GFP output. To test this, a representative *in silico* realization is shown in the left inset of Fig. 5(A) with a zoom-in into the region marked by the dashed line box shown in the main panel. Cell-cell contact lengths for individual synNotch cells (colored green/black) along the border are marked in different colors showing notable differences in lengths and the number of ligand cells (colored blue) in contact. Note that some synNotch cells make contact with a single ligand cell (see Cell #1 and Cell #3 in Fig. 5(A)) while Cell #4 makes contact with 4 distinct ligand cells due to its shape and position within the clone.

Even though the GFP synthesis rate S is constant for all the synNotch cells along the border, we observe a linear dependence between the cell-cell contact length and GFP output (Fig. 5(B-D)). Differences in the output emerge due to shorter and longer contact lengths varying from $0 - 15\mu m$, Fig. 5(B-D). This can be understood by considering the equation governing the dynamics of GFP signal output in synNotch cells (Eq. (3)). The term representing intracellular GFP synthesis depends not only on S but also on $l_{\alpha\beta}$ (length of the ligand-synNotch cell-cell junction).

In line with our predictions, we anticipate that in a growing *Drosophila* wing disc, cell growth and cell elongation, resulting in apical surface expansion, and orientation of cell division act collectively to give rise to the observed variation in interface cell bond length. To check this we analyzed and segmented *in vivo* images of wing disc epithelial cells exhibiting synNotch response (see Fig. 5 (E-F)). We compared the total GFP signal intensity to the synNotch cell perimeter and find that there is a strong correlation between the two ($R^2 = 0.4$ and linear trendline in Fig. 5 (G)). The observed correlation of output intensity with contact length strongly supports a model in which larger contact length results in more signaling with large variations in the output.

The active cell growth process and the associated cell mechanical properties, therefore, have direct implications on the output spatiotemporal patterns obtained from cell-cell

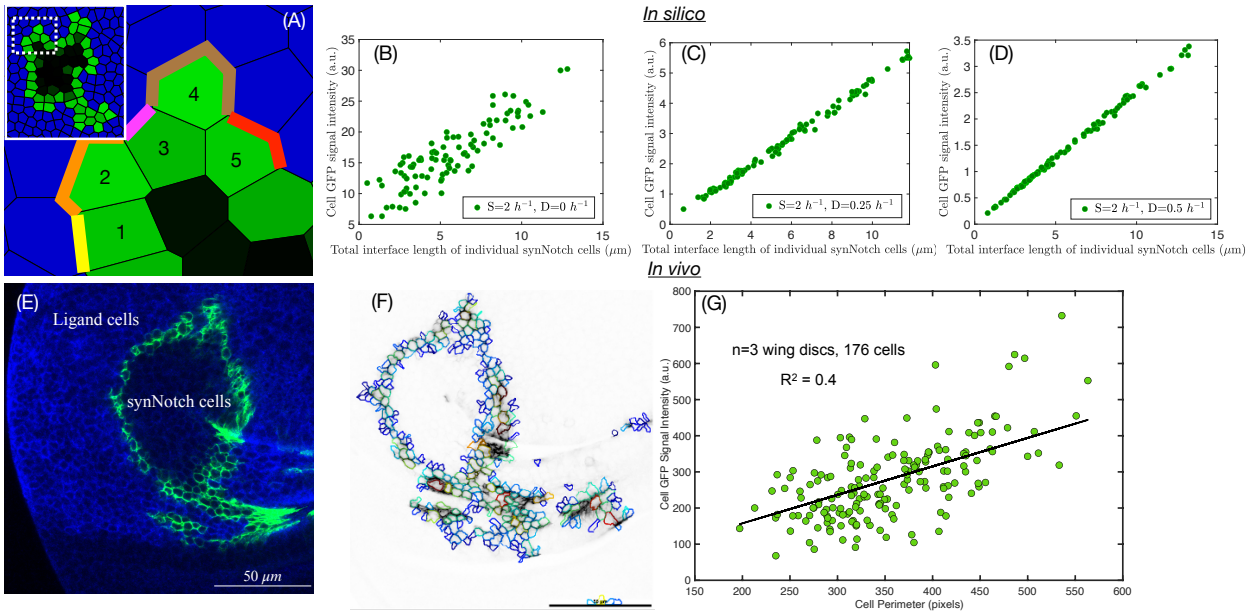

FIG. 5: **GFP output varies in proportion to cell-cell contact length between synNotch and ligand cells. (A)** Cell division and cell area growth give rise to variations in the total contact lengths. The entire synNotch clone is visible in the left inset, and the zoom-in view in the main panel. Individual cells are labeled 1 through 5. **(B-D)** GFP output intensity in the border synNotch increases with the total contact length between synNotch and ligand cells irrespective of the decay rates (B) $D = 0h^1$,(C) $0.25h^1$ and (D) $0.5h^1$. Cell #1 has a smaller contact length with a ligand cell while Cell #4 has a larger contact length. **(E)** *In vivo* confocal image of the wing disc with synNotch cell clone and ligand cells in blue. **(F)** Cell segmentation generated using Cell Profiler[44,45] was manually filtered to remove misidentified cells (see Materials and Methods, Section 5) to obtain cell perimeter versus integrated GFP intensities. **(G)** As predicted, the GFP intensity increases with cell size. Data was obtained from 176 individually identified synNotch cells from 3 wing discs.

contact-based signaling. As mechanical forces generated by myosin, actin[46] together with cell-cell adhesion molecules[47] can regulate the cell-cell contact length, our results provide insight into how cell mechanical properties could impact signal output in growing clones[48,49]. While molecular scale variabilities such as temporal differences in the level of receptor activation may also impact synNotch output[50], we show that variation in cell-cell junction length is the dominant physical parameter that determines juxtacrine signal output.

DISCUSSION

Here, we implement a combined computational and experimental approach and elucidate the emergent spatiotemporal patterns of synNotch output in a growing tissue. Despite the complexity underlying synthetic cell communication *in vivo*, our minimal computational

model captures key experimentally observed features of the output patterns that emerge following synNotch activation in growing *Drosophila* wing discs. Specifically, we show that the synthetic signal output in expanding clones self-organize into complex patterns determined by the dynamics of cell growth and division on the basis of the following key parameters: (i) contact length dependent synNotch activation, (ii) cell area growth and division, and (iii) output synthesis and degradation. Importantly, we show that the clone shape is an important determinant of juxtacrine signal output and exhibit a spatially graded output profile, characterized by an exponentially decaying function. Consistent with our model predictions, *in vivo* experiments show spatial exponential gradient of GFP fluorescence across the synNotch cell clone with several cells away from the interface exhibiting detectable synNotch output. Such graded profiles across a tissue are well defined for morphogens, such as decapentaplegic (Dpp) and Wingless (Wg, a Wnt homolog), that diffuse from a population of source cells[13]. However, regarding the question of whether an output gradient can be established in the absence of diffusible signals, we provide a plausible mechanism for spatially graded juxtacrine signal outputs. When a responding synNotch cell divides, the output is divided equally between the daughter cells making it possible to have daughter cells that continue to exhibit output while not in contact with the ligand cells. Multiple rounds of cell division can produce responding cells several cell diameters into the clone, with the output decaying exponentially as each division halves the output. Propagation of a juxtacrine signal output may well be a general feature of contact-mediated signaling in growing tissues like the wing and resembles gradients formed over a greater distance by morphogens. For instance, the diffusible morphogens Dpp and Wg normally elicit growth and transcriptional responses over 30 cell diameters away from their source. Interestingly, when tethered or restricted to the surface of producing cells, transcriptional responses can still be detected in cells several cell diameters away from the signal-sending cells[21]. This may arise due to a similar mechanism as we propose here - due to cell division-driven displacement of cells. Such activity might contribute to the rescue of the development of animals where the only form of Wg is cell membrane tethered[51].

Alternatively, it is possible that an output several cell diameters from the clonal interface may be induced by other means. For instance, basal cell extensions in the epithelium of the fly notum can support long-range Delta/Notch signaling over several cell diameters[52] and there is evidence that cell extensions or cytonemes that extend basally across multiple

cell lengths in the wing imaginal disc can act as signaling platforms for the morphogen Hedgehog[53,54]. Our model does not include such long range contact-based signaling, and restricts signaling to synNotch cells immediately adjacent to the ligand cells. Nevertheless, the model produces patterns where there is a variable but significant number of cells that produce an output away from the ligand interface. Our results therefore suggest that cell proliferation can account for the long range of output.

Our results imply that the overall clone shape is likely important in determining the juxtacrine signal output in proliferating tissues, a consequence of the signal output being proportional to the cell-cell contact length [16]. As such, points of geometric inflection in the clone can substantially change the extent of cell-cell contact and in turn the strength of the synNotch output. We show that the clone morphology becomes highly irregular with growth which is a function of the tension of the cell bonds at the interface[48]. This has important implications on future strategies for building synthetic circuits and will need to be factored in to achieve desired synNotch outputs in proliferating tissues. In cases where the synNotch response affects proliferation, more sophisticated mathematical models will be required that can accurately predict the impact on signal transduction due to tissue growth and cell rearrangements[55–58]. Overall, our multi-scale approach, linking the intracellular biochemical processes of GFP synthesis and degradation, together with cell and tissue level growth processes provides a quantitative assay to elucidate complex emergent patterns underlying juxtacrine signaling.

MATERIALS AND METHODS

1. *Drosophila* Method Details

***Drosophila* Transgenes:** Fly stocks were maintained at 25°C on standard corn food, and all experiments were performed at 25°C on standard corn food. All ligand and receptor coding sequences, with the exception of FSHα, were inserted into a modified form of *pUAST-attB* (www.flyc31.org) that contains a single Flp Recombinase Target (FRT, $>$) positioned between the UAS promoter and the coding sequence, and the resulting $UAS > FSH-Delta$ and $UAS > FSHR-synNotch$ transgenes were inserted at a single genomic docking site, $attP-86Fb$ located on the right arm of the third chromosome and were oriented so that the promoter is centromere proximal to the coding sequence[59]. A single $UAS.FSH\alpha$, transgene inserted by conventional P-element mediated transformation onto the X chromosome was used in all experiments. The FSH chimeric form of Delta is described in detail in Ref.[31] . Briefly, the native extracellular domain of Delta was replaced in its entirety by the β subunit of human Follicle Stimulation Hormone (FSHβ)[60] and an HRP tag was inserted immediately downstream of the C-terminal YCSFGEMKE sequence of FSHβ and immediately upstream of the Dl transmembrane domain. In all experiments, FSHα was co-expressed with the FSHβ-Dl protein to reconstitute FSH, which is an FSHα/FSHβ heterodimer (for simplicity, we refer to the ligand as the FSH-Delta chimera and do not include the HRP tag in its designations). The FSHR-synNotch form of Notch is based on the FSHR-A2-Notch receptor described in detail[59]. Briefly the amino-terminal Epidermal Growth Factor (EGF) Repeat containing portion of the native extracellular domain of N was replaced by the ectodomain of FSHR. The extracellular domain was tagged by the insertion of mCherry just upstream of the juxtamembrane A2 domain. The NRR of Notch was replaced with the force sensitive region of von Willibrand Factor A2 domain. Previous work has shown that this domain acts as a force sensor in the same way as the NRR[59]. The additional change to FSHR-A2-Notch to form FSHR-synNotch replaced the cytosolic domain of FSHR-A2-Notch with the LexA-VP16 trascription factor[61] . The join between Notch and Lex A is as follows (the Notch sequence is in uppercase): VITGIILVIIALAFFGMVLSTQRKRsgppkaltarqqevfdlir. Complete DNA sequences for both the ligand and receptor are available on request.

Analysis of signaling between FSH-Delta and FSHR-synNotch expressing cells
Signaling between FSH-Delta and FSHR-Notch cells was established using Mosaic Analysis by Promoter Swap (MAPS; see[31] for detailed description). In brief, mitotic recombination across the FRTs in cells transheterozygous for UAS>transgenes is induced in the presence of a *nub.Gal4* driver that acts in the developing wing. Upon the appropriate segregation of the recombined chromatid arms at the 4 strand stage, populations of FSH-Delta and FSHR-synNotch expressing cells were generated; the FSH-Delta expressing cells are marked by staining for the HRP epitope tag (blue in all of the Figures), and the dedicated FSHR-synNotch expressing cells are marked "black" by the absence of HRP expression. Receptor activation occurs at the interface between the cells that express FSH-Delta and those that express solely the receptor[59]. Here this was monitored by assaying for a GFP output, since FSHR-synNotch activation results in the translocation of the LexA-VP16 transcription factor to the nucleus and expression of a transgene composed of the LexO promoter followed by a fusion of the surface protein CD2 followed by GFP (LexAop rCD2::GFP, Bloomington Stock Center). To induce mosaics by promoter swap, first or second instar larvae of the appropriate genotype ($hsp70.flp\ UAS.FSH\alpha/hsp70.flp$ or $Y; nub.Gal4/LexAop\ \ rCD2::GFP;\ UAS>FSH-Delta/UAS>FSHR-synNotch$) were heat shocked at 33°C for 20 minutes and wing discs from mature third instar larvae were dissected, fixed, stained for HRP expression and mounted for confocal microscopy [commercially available Rabbit anti-HRP (Abcam ab34885, 1/1000) antisera were used in combination with Alexa 633 conjugated labelled secondary antisera following standard protocols, e.g., as in[31]]. The native fluorescence of the GFP was also visualized in these preparations.

2. Vertex based modeling framework for synNotch induced gene expression

We use the vertex model to represent the *Drosophila* wing disc epithelium as a two dimensional cell layer. Using a cell-based computational framework, Virtual Leaf[62,63], we simulate coupled vertex and chemical dynamics we implemented. The two-dimensional description is a good approximation for the wing disc epithelium if changes in cell height are assumed to be negligible, Fig. 1(D). Cells in this epithelial monolayer are represented as a network of interconnected polygons (edges as straight lines connecting vertices). The

configuration of each individual cell, and thus of the whole network, is characterized by the positions of the vertices, and the connections between them. Assuming cell shape relaxations occur at timescales much faster than the cell division, the stable network configuration is determined by the minima of the energy function,

$$\mathcal{E} = \sum_{\alpha} (K_A (A_\alpha - A_0)^2 + K_P (P_\alpha - P_0)^2), \tag{2}$$

where, A_α and P_α are the area and perimeter of cell α, respectively. A_0 and P_0 are the preferred area and perimeter of cell α. The summation is over all cells $\alpha = 1 \cdots N(t)$, where $N(t)$ is the total number of cells at time t. The first term describes the cell area elasticity with an elastic coefficient K_A which results from cell volume incompressibility and the cell monolayer's resistance to height fluctuations. The second term describes the stiffness of the cell perimeter P_α with an elastic constant, K_P, and it results from two processes: contractility of the actomyosin subcellular cortex and effective cell membrane tension due to cell-cell adhesion and cortical line tension. The energy function described by Eq. (2) is widely used to study tissue mechanics during morphogenesis[64,65].
A detailed description of the VirtualLeaf vertex modeling framework, which we have adapted here, is given in Ref.[62]. The shape of a cell, and thus the whole tissue, is determined by the force balanced state, i.e., the state in which the forces, described in the energy function $\mathcal{E}$ given by Eq.(2), acting on each node have sufficiently balanced out. The simulation of this vertex model employs Monte Carlo based 'Metropolis dynamics' method to alter the positions of the vertices until the energy function, given by Eq.(2), is minimized such that all interfacial tensions are balanced by cellular pressures[62]. We assume the mechanical properties of all the cells of both the cell types in the tissue, i.e., ligand and receptor-expressing synNotch cells, to be homogeneous and constant. The values of the model parameters are listed in the Table (I).

3. Dynamics of GFP signal pattern in synNotch cells

To characterize the spatiotemporal pattern of synNotch induced GFP output in the *Drosophila* wing disc, in addition to the dynamics of cell shape and cell division, we incorporate a dynamic equation for the change in the number of GFP molecules in a synNotch cell. The cell GFP signal intensity at any time t in our model is proportional to

the total number of GFP molecules in the cell at that time. Our modeling framework thus gives rise to a coupling between three timescales at the scale of a single cell, namely, the intracellular GFP synthesis rate, the rate of intracellular GFP degradation and the rate of cell division.

In our model, the wing disc epithelium consists of two types of cells, namely, synthetic ligand expressing cells and synthetic Notch receptor expressing cells (which we refer to as synNotch cells). The ligand expressing cells are assigned a label or cell type of 0 and the synNotch receptor cells are assigned a label or cell type of 1. This binary-type quantity T is a function of cell α, where α is the cell index, $i \in 1 \ldots N$. T takes the value $T(\alpha) = 0$ if the cell α is a ligand expressing cell and $T(\alpha) = 1$ for a synNotch receptor cell, Fig. 1(A). The total number of cells at any given time point is $N(t) = N_{(T=0)} + N_{(T=1)}$, where $N_{(T=0(1))}$ is the total number of cells of type $T = 0(1)$. We assume that the whole wing disc is fully characterized as comprising of type 0 and type 1 cells. The cell identity, $T(\alpha) = 0$ or 1, assigned to a cell is conserved across cell division events. Therefore, when a cell α of type $T(\alpha) = 0$, i.e., a ligand expressing cell, divides, it produces two daughter cells, both of which are of cell type 0. Similarly, when a cell of cell type $T(\alpha) = 1$, i.e., a synNotch cell, divides, it produces two daughter cells, both of which are cells of cell type 1. We propose that the dynamics of GFP output (G_α) as a function of t is given by,

$$\frac{dG_\alpha(t)}{dt} = S \sum_\beta \frac{l_{\alpha\beta}(t)(1 - \delta_{T(\alpha),T(\beta)})}{P_\alpha(t)} - DG_\alpha(t). \tag{3}$$

The first term on the right hand side of Eq.(3) describes GFP synthesis at the rate $S(h^{-1})$ in synNotch cells. The summation is over all cells β neighboring a cell α. GFP is synthesized only in those synNotch receptor cells that are adjacent to the synthetic ligand expressing cells, i.e., synNotch receptor cells which share an edge or a cell bond with the ligand expressing cells. This condition is ensured in the model by the kronecker delta function $\delta_{T(\alpha),T(\beta)}$, which assumes the value 0 if the Notch cell α and its adjacent cell β are of different types, i.e., $(T(\alpha) \neq T(\beta))$, and, the value 1 if they are of the same type, i.e., $(T(\alpha) = T(\beta))$. With this condition, GFP synthesis is restricted to only those cells that share a cell-cell junction with synthetic ligand expressing cells. We propose that GFP output in a synNotch cell is proportional to the length of the cell bond, $l_{\alpha\beta}$ (μm) shared with its adjacent synthetic ligand expressing cell, and normalized to the overall perimeter P_α (μm) of the synNotch cell α at time t. The second term on the right hand of Eq.(3)

accounts for the degradation of GFP in the synNotch cell α at a constant rate of D (h^{-1}). Now, we briefly describe the non-dimensionalization of Eq.(3). By multiplying both sides of the Eq.(3) by $t^* = 1h$ we can write the dimensionless form of Eq.(3) as,

$$\frac{dG_\alpha}{d\tilde{t}} = \tilde{S}\sum_\beta \frac{\tilde{l}_{ij}(1-\delta_{T(\alpha),T(\beta)})}{\tilde{P}_\alpha} - \tilde{D}G_\alpha \tag{4}$$

where, $\tilde{D} = Dt^*$, $\tilde{S} = St^*$, $\tilde{P} = \frac{P}{\sqrt{A^*}}$, and $\tilde{l}_{ij} = \frac{l_{ij}}{\sqrt{A^*}}$.

5. Analytical derivation showing dependence of the total synNotch GFP expression on the shape of the synNotch cell colony

The time dependent dynamics of the total GFP expression in the whole synNotch cell colony is described by the following equation,

$$\frac{dG(t)}{dt} = S\sum_{\alpha=1}^{N(t)}\sum_\beta \frac{l_{\alpha\beta}(t)(1-\delta_{T(\alpha),T(\beta)})}{P_\alpha(t)} - DG(t) \qquad . \tag{5}$$

If we assume each individual cell within the synNotch cell colony has roughly the same perimeter which is $P_\alpha = \bar{P}$ then,

$$\frac{dG(t)}{dt} \sim \frac{S}{\bar{P}}\sum_{\alpha=1}^{N(t)}\sum_\beta l_{\alpha\beta}(t)(1-\delta_{T(\alpha),T(\beta)}) - DG(t) \qquad . \tag{6}$$

Let us introduce an average cell shape factor $\bar{f} = \frac{\bar{P}}{\sqrt{\bar{A}}}$, where $\bar{A}$ is the average single cell area and is defined as $\bar{A} = A_m/N_m$, with A_m being the total area of the whole synNotch cell colony, and N_m being the total number of synNotch cells in that colony in the time interval $t \in [\tau_m, \tau_{m+1}]$ between two succesive cell division events.

$$\frac{dG(t)}{dt} \sim \frac{S\sqrt{N_m}}{\bar{f}\sqrt{A_m}}\sum_{\alpha=1}^{N(t)}\sum_\beta l_{\alpha\beta}(t)(1-\delta_{T(\alpha),T(\beta)}) - DG(t) \qquad . \tag{7}$$

The double summation in Eq. (7) actually results in the perimeter of the whole synNotch cell colony in the time interval $t \in [\tau_m, \tau_{m+1}]$, which we will denote by P_m.

$$\frac{dG(t)}{dt} \sim \frac{S\sqrt{N_m}}{\bar{f}\sqrt{A_m}}P_m - DG(t) \qquad . \tag{8}$$

The factor $\frac{P_m}{\sqrt{A_m}}$ in Eq. (8)is the shape factor of the whole synNotch cell colony at time t which we will denote F_m.

$$\frac{dG(t)}{dt} \sim \frac{SF_m}{\bar{f}}\sqrt{N_m} - DG(t) \qquad . \tag{9}$$

The above equation can also be written in terms of circularity of the whole synNotch clone. The circularity parameter is related to the shape factor in the following manner, $F_m = 2\sqrt{\frac{\pi}{C}}$,

$$\frac{dG(t)}{dt} \sim \frac{2S}{\bar{f}}\sqrt{\frac{\pi N_m}{C_m}} - DG(t) \qquad . \tag{10}$$

Therefore, we predict that when the circularity of the synNotch clone is small (at lower values of C_m), we expect the source term contribution to be effectively larger. This would lead to an enhanced synNotch output.

4. Rules governing cell growth and division

Each cell in the *in silico* tissue is fixed to the same base area, A_b. Our initial condition is such that all the cells are set to $A_\alpha = A_b = 50$, where α is the cell index. At $t = 0$, the preferred area A_0 of all the cells is equal to the base area. The dimensionless value of 50 for the cell area in the model corresponds to an experimental value of $10\mu\text{m}^2$. To implement cell area growth over time, as described in[62], the cell preferred area is increased in the next time step $t + \delta t$ as,

$$A_0(t + dt) = A_0(t) + g_0 dt \tag{11}$$

where, g_0 is the value by which the cells preferred area is incremented in the next time step. The cell area at each time step is relaxed quasi-statically to the preferred area, which results in an irreversible increase in the cell area over time. Over time, when the area of a cell A_α is double the base area A_b then the cell divides over its short axis, Fig. 1(D-iv). Right after division, the preferred area of the divided cell is reset to $A_0 = A_b = 50$. As a result the area of each daughter cell, the instant after cell division, is relaxed to $A_0 = A_b$. Since the cell divides when its area A_α reaches a value which is twice the base area of the cell A_b, which occurs in the time duration τ,

$$\frac{A_0}{\tau} = g_0, \tag{12}$$

in our simulations we chose a timescale such that 1 relaxation step that minimizes the energy function E, given by Eq. (2), for the preferred $A_0(t)$ at the time t, corresponds to 1 h. We set $A(t) = A_0$, where $A_0 = 10\mu m^2$ is the typical base area of a cell in the wing disc

epithelium. The typical time τ over which a wing disc epithelium cell divides is equal to 10 h. Hence, $g_0 = 1\mu m^2/h$ is the typical cell area growth rate. By dividing and multiplying both sides of Eq.(12) by a unit area $A^* = 0.2\mu m^2$ and a unit time $t^* = 1h$, respectively, we obtain,

$$\frac{\tilde{A}_0}{\tilde{\tau}} = \tilde{g}_0 \tag{13}$$

We chose the cell base area as $\tilde{A}_0 = 50$, which corresponds to the experimental value of $10\mu m^2$, and cell division time $\tilde{\tau} = 10$, which is equivalent to 10h, implying that $\tilde{g}_0 = 5$.

5. Bio-image analysis

For measuring the cell perimeter and the corresponding synNotch output (GFP) from experimental images, we used the free and open-source bioimage analysis software CellProfiler[44] and CellProfiler Analyst[45]. The provisions within CellProfiler for automated cell segmentation was used to identify the cell membrane borders of individual cells in images that we analyzed. The difference in the GFP intensity between the bright cell membrane of a responding cell and the corresponding dark cytoplasm of the cell interior was used to segment out the cell membrane of each of the identified individual synNotch cells. Intensity of GFP response along the cell membrane was measured for each cell together with the cell shape parameter quantifications. These measurements were then filtered using CellProfiler Analyst, where a machine learning algorithm selected the misidentified cells. The CellProfiler Analyst was imperfect in its ability to completely filter out all misidentifications, so further manual filtering was required to obtain the results shown.

Parameter values

TABLE I: Model parameters, their meaning, dimensionless values and equivalent magnitude in experimental units

Model parameter	Description	Values (Dimensionless)	Experimental values
A_b	Cell base area	50	$\sim 10\mu\text{m}^2$ [66]
A_0	Range of cell preferred area	[50-100]	$[10-20]\mu m^2$
P_0	Cell preferred perimeter	25	$\sim 11\ \mu\text{m}$[66]
K_A	Area elastic constant	500	
K_P	Perimeter elastic constant	100	
g_0	Cell area growth rate	5	$1\ \mu\text{m}^2/h$
S	Rate of cellular GFP output	2	$0.5\ \text{h}^{-1}$
D	Rate of cellular GFP degradation	[0-0.5]	$\sim$[0-0.5] h^{-1} [40,67]
dt	Time step	1	1 h

ACKNOWLEDGMENTS

A.M.K acknowledges support from the College of Science and Mathematics at Augusta University (AU). P.L. acknowledges support from NICHD (R21HD107414), the Roy and Diana Vagelos Precision Medicine Award and the Research Scholarship & Creativity Activity Program at AU. P.L. thanks Gary Struhl for assistance with transgene design and Olivia Mosley for technical support. A.M.K and P.L. acknowledges support from AU CURS Summer Scholars Program. We thank Jessica Hoffmann, Sumit Sinha, and Xin Li for their valuable comments on the manuscript.

REFERENCES

[1]Ruder, W. C., Lu, T. & Collins, J. J. Synthetic biology moving into the clinic. *Science* **333**, 1248–1252 (2011).

[2]Santorelli, M., Lam, C. & Morsut, L. Synthetic development: building mammalian multicellular structures with artificial genetic programs. *Current opinion in biotechnology* **59**, 130–140 (2019).

[3]Liu, A. P. *et al.* The living interface between synthetic biology and biomaterial design. *Nature materials* **21**, 390–397 (2022).

[4]Davies, J. A. & Cachat, E. Synthetic biology meets tissue engineering. *Biochemical Society Transactions* **44** (2016).

[5]Davies, J. Using synthetic biology to explore principles of development. *Development (Cambridge)* **144** (2017).

[6]Tiemeijer, L. A., Sanlidag, S., Bouten, C. V. & Sahlgren, C. M. Engineering tissue morphogenesis: taking it up a notch. *Trends in Biotechnology* (2022).

[7]Muskavitch, M. A. Delta-notch signaling and drosophila cell fate choice. *Developmental biology* **166**, 415–430 (1994).

[8]Huizar, F., Soundarrajan, D., Paravitorghabeh, R. & Zartman, J. Interplay between morphogen-directed positional information systems and physiological signaling. *Developmental Dynamics* **249**, 328–341 (2020).

[9]Toda, S. *et al.* Engineering synthetic morphogen systems that can program multicellular patterning. *Science* **370** (2020).

[10]Stapornwongkul, K. S., de Gennes, M., Cocconi, L., Salbreux, G. & Vincent, J.-P. Patterning and growth control in vivo by an engineered gfp gradient. *Science* **370**, 321–327 (2020).

[11]Grant, P. K. *et al.* Interpretation of morphogen gradients by a synthetic bistable circuit. *Nature Communications* **11** (2020).

[12]Bocci, F., Onuchic, J. N. & Jolly, M. K. Understanding the principles of pattern formation driven by notch signaling by integrating experiments and theoretical models. *Frontiers in Physiology* **11** (2020).

[13]Simsek, M. F. & Ozbudak, E. M. Patterning principles of morphogengradients. *Open Biology* **12** (2022).

[14]Turing, A. M. The chemical basis of morphogenesis. *Philosophical Transactions of the Royal Society of London. Series B, Biological Sciences* **237**, 37–72 (1952). URL `http://www.jstor.org/stable/92463`.

[15]Wartlick, O. *et al.* Dynamics of dpp signaling and proliferation control. *Science* **331** (2011).

[16]Shaya, O. *et al.* Cell-cell contact area affects notch signaling and notch-dependent patterning. *Developmental Cell* **40** (2017).

[17]Barbier, I., Perez-Carrasco, R. & Schaerli, Y. Controlling spatiotemporal pattern formation in a concentration gradient with a synthetic toggle switch. *Molecular Systems Biology* **16** (2020).

[18]Stopka, A., Boareto, M. & Iber, D. Cell-based simulations of notch-dependent cell differentiation on growing domains. *bioRxiv* 859363 (2019).

[19]Lawrence, P. A. & Struhl, G. Morphogens, compartments, and pattern: Lessons from drosophila? *Cell* **85** (1996).

[20]Rogers, K. W. & Schier, A. F. Morphogen gradients: From generation to interpretation. *Annual Review of Cell and Developmental Biology* **27** (2011).

[21]Zecca, M. & Struhl, G. A unified mechanism for the control of drosophila wing growth by the morphogens decapentaplegic and wingless. *PLoS Biology* **19** (2021).

[22]Rodríguez, A. D. V., Didiano, D. & Desplan, C. Power tools for gene expression and clonal analysis in drosophila. *Nature Methods* **9** (2012).

[23]Morata, G. & Lawrence, P. An exciting period of drosophila developmental biology: Of imaginal discs, clones, compartments, parasegments and homeotic genes". *Developmental Biology* **484** (2022).

[24]Tripathi, B. K. & Irvine, K. D. The wing imaginal disc. *Genetics* **220**, iyac020 (2022).

[25]Bryant, P. J. & Simpson, P. Intrinsic and extrinsic control of growth in developing organs. *The Quarterly review of biology* **59** (1984).

[26]Lim, W. A. The emerging era of cell engineering: Harnessing the modularity of cells to program complex biological function. *Science* **378**, 848–852 (2022).

[27]Du, P. *et al.* De novo design of an intercellular signaling toolbox for multi-channel cell–cell communication and biological computation. *Nature communications* **11**, 4226 (2020).

[28]Gazave, E. *et al.* Origin and evolution of the notch signalling pathway: An overview from eukaryotic genomes. *BMC Evolutionary Biology* **9** (2009).

[29]Zhou, B. *et al.* Notch signaling pathway: architecture, disease, and therapeutics. *Signal Transduction and Targeted Therapy* **7** (2022).

[30]Langridge, P. D., Diaz, A. G., Chan, J. Y., Greenwald, I. & Struhl, G. Evolutionary plasticity in the requirement for force exerted by ligand endocytosis to activate c. elegans notch proteins. *Current Biology* **32**, 2263–2271 (2022).

[31]Langridge, P. D. & Struhl, G. Epsin-dependent ligand endocytosis activates notch by force. *Cell* **171** (2017).

[32]Lecuit, T. & Le Goff, L. Orchestrating size and shape during morphogenesis. *Nature* **450**, 189–192 (2007).

[33]Mao, Y. *et al.* Differential proliferation rates generate patterns of mechanical tension that orient tissue growth. *The EMBO journal* **32**, 2790–2803 (2013).

[34]Miller, C. J. & Davidson, L. A. The interplay between cell signalling and mechanics in developmental processes. *Nature Reviews Genetics* **14**, 733–744 (2013).

[35]Heller, E. & Fuchs, E. Tissue patterning and cellular mechanics. *Journal of Cell Biology* **211**, 219–231 (2015).

[36]Fletcher, A. G., Osterfield, M., Baker, R. E. & Shvartsman, S. Y. Vertex models of epithelial morphogenesis. *Biophysical Journal* **106**, 2291–2304 (2014).

[37]Gruening, M. *et al.* Automatic actin filament quantification and cell shape modeling of osteoblasts on charged ti surfaces. *Applied Sciences (Switzerland)* **11** (2021).

[38]Wolpert, L. Positional information and the spatial pattern of cellular differentiation. *Journal of Theoretical Biology* **25**, 1–47 (1969).

[39]Gregor, T., Wieschaus, E. F., McGregor, A. P., Bialek, W. & Tank, D. W. Stability and nuclear dynamics of the bicoid morphogen gradient. *Cell* **130** (2007).

[40]Halter, M., Tona, A., Bhadriraju, K., Plant, A. L. & Elliott, J. T. Automated live cell imaging of green fluorescent protein degradation in individual fibroblasts. *Cytometry Part A* **71** (2007).

[41]He, L., Binari, R., Huang, J., Falo-Sanjuan, J. & Perrimon, N. In vivo study of gene expression with an enhanced dual-color fluorescent transcriptional timer. *Elife* **8** (2019).

[42]Milán, M., Campuzano, S. & García-Bellido, A. Cell cycling and patterned cell proliferation in the wing primordium of drosophila. *Proceedings of the National Academy*

of Sciences of the United States of America **93** (1996).

[43]Micchelli, C. A. & Blair, S. S. Dorsoventral lineage restriction in wing imaginal discs requires notch. *Nature* **401** (1999).

[44]Stirling, D. R. *et al.* Cellprofiler 4: improvements in speed, utility and usability. *BMC bioinformatics* **22**, 1–11 (2021).

[45]Jones, T. R. *et al.* Cellprofiler analyst: data exploration and analysis software for complex image-based screens. *BMC bioinformatics* **9**, 1–16 (2008).

[46]Cavanaugh, K. E., Staddon, M. F., Banerjee, S. & Gardel, M. L. Adaptive viscoelasticity of epithelial cell junctions: from models to methods. *Current opinion in genetics & development* **63**, 86–94 (2020).

[47]Huebner, R. J. *et al.* Mechanical heterogeneity along single cell-cell junctions is driven by lateral clustering of cadherins during vertebrate axis elongation. *Elife* **10**, e65390 (2021).

[48]Aliee, M. *et al.* Physical mechanisms shaping the drosophila dorsoventral compartment boundary. *Current Biology* **22**, 967–976 (2012).

[49]Umetsu, D. Cell mechanics and cell-cell recognition controls by toll-like receptors in tissue morphogenesis and homeostasis. *Fly* **16**, 233–247 (2022).

[50]Nandagopal, N. *et al.* Dynamic ligand discrimination in the notch signaling pathway. *Cell* **172**, 869–880 (2018).

[51]Alexandre, C., Baena-Lopez, A. & Vincent, J.-P. Patterning and growth control by membrane-tethered wingless. *Nature* **505**, 180–185 (2014).

[52]Hunter, G. L. *et al.* A role for actomyosin contractility in notch signaling. *BMC Biology* **17** (2019).

[53]Bischoff, M. *et al.* Cytonemes are required for the establishment of a normal hedgehog morphogen gradient in drosophila epithelia. *Nature Cell Biology* **15** (2013).

[54]Zhang, C. & Scholpp, S. Cytonemes in development. *Current Opinion in Genetics and Development* **57**, 25–30 (2019).

[55]Malmi-Kakkada, A. N., Li, X., Samanta, H. S., Sinha, S. & Thirumalai, D. Cell growth rate dictates the onset of glass to fluidlike transition and long time superdiffusion in an evolving cell colony. *Physical Review X* **8**, 021025 (2018).

[56]Sinha, S., Malmi-Kakkada, A. N., Li, X., Samanta, H. S. & Thirumalai, D. Spatially heterogeneous dynamics of cells in a growing tumor spheroid: Comparison between theory and experiments. *Soft Matter* **16**, 5294–5304 (2020).

[57]Sinha, S. & Malmi-Kakkada, A. N. Inter-particle adhesion regulates the surface roughness of growing dense three-dimensional active particle aggregates. *J. Phys. Chem. B* **125**, 10445–10451 (2021).

[58]Malmi-Kakkada, A. N., Sinha, S., Li, X. & Thirumalai, D. Adhesion strength between cells regulate non-monotonic growth by a biomechanical feedback mechanism. *Biophysical Journal* **121**, 1–11 (2022).

[59]Langridge, P. D. & Struhl, G. Epsin-dependent ligand endocytosis activates notch by force. *Cell* **171**, 1383–1396 (2017).

[60]Fan, Q. R. & Hendrickson, W. A. Structure of human follicle-stimulating hormone in complex with its receptor. *Nature* **433** (2005).

[61]Kidd, S., Lieber, T. & Young, M. W. Ligand-induced cleavage and regulation of nuclear entry of notch in drosophila melanogaster embryos. *Genes and Development* **12** (1998).

[62]Merks, R. M., Guravage, M., Inzé, D. & Beemster, G. T. Virtualleaf: An open-source framework for cell-based modeling of plant tissue growth and development. *Plant Physiology* **155** (2011).

[63]Kneuper, I. *et al.* Auxin biosynthesis and cellular efflux act together to regulate leaf vein patterning. *Journal of Experimental Botany* (2020).

[64]Erdemci-Tandogan, G. & Manning, M. L. Effect of cellular rearrangement time delays on the rheology of vertex models for confluent tissues. *PLoS Computational Biology* **17** (2021).

[65]Wang, X. *et al.* Anisotropy links cell shapes to tissue flow during convergent extension. *Proceedings of the National Academy of Sciences of the United States of America* **117** (2020).

[66]Romanova-Michaelides, M. *et al.* Morphogen gradient scaling by recycling of intracellular dpp. *Nature* **602** (2022).

[67]He, L., Binari, R., Huang, J., Falo-Sanjuan, J. & Perrimon, N. In vivo study of gene expression with an enhanced dual-color fluorescent transcriptional timer. *eLife* **8** (2019).